Emergence of highly-ordered hierarchical nanoscale aggregates on electrostatic binding of self-assembled multivalent (SAMul) cationic micelles with polyanionic heparin

Vania M. P. Vieira,[a] Ville Liljeström,[b] Paola Posocco,[c] Erik Laurini,[c] Sabrina Pricl,[c] Mauri A. Kostiainen[b,*] and David K. Smith[a,*]

a: Department of Chemistry, University of York

b: Biohybrid Materials, Department of Biotechnology and Chemical Technology, Aalto University

c: Simulation Engineering (MOSE) Laboratory, Department of Engineering and Architectures (DEA), University of Trieste, Trieste, 34127, Italy

SUPPORTING INFORMATION

Contents

1. General Experimental Methods

All compounds required in synthesis were purchased from commercial sources and were used directly without any further purification. *N*,*N*-di-(3-aminopropyl)-*N*-methylamine (DAPMA) was mono-Boc protected using methods adapted from those in the literature for mono-amine protection and had data fully characteristic of its structure. C16-DAPMA was synthesised according to literature methods.[1] Thin layer chromatography (TLC) was performed on Merck aluminium-backed plates coated with 0.25 nm silica gel 60. Preparative gel permeation chromatography (GPC) was performed on Biobeads SX-1 supplied by Bio-Rad. NMR spectra were recorded on a JEOL ECX400 spectrometer (^{1}H 400 MHz, ^{13}C 100 MHz). ESI mass spectra were recorded on a Bruker Daltonics MicroTOF mass spectrometer. Infrared spectra were recorded on Perkin Elmer Spectrum Two FT-IR spectrometer. Fluorescence spectra were obtained with a Hitachi F-4500 fluorimeter. UV-Vis absorvance was recorded on a Shimadzu UV-2401PC spectrophotometer. TEM images were obtained using a FEI Tecnai 12 Bio TWIN operated at 120 kV. DLS and zeta potential measurements were recorded on a Zetasizer Nano ZS. SAXS was performed using a setup consisting of a rotating anode microfocus X-ray source (Bruker), a Montel Multilayer focusing monochromator (Incoatec) and four collimating slits (JJ X-ray).

2. Synthesis and Characterization of Compounds

Boc-Protected C14-DAPMA. Myristic acid (1.00 g, 4.4 mmol) was dissolved in CH_2Cl_2 (65 mL). TBTU (1.41 g, 4.4 mmol) and Et_3N (5.4 mL) were added to the mixture and it was stirred for 5 min at room temperature. Mono-Boc-Protected DAPMA (1.08 g, 4.4 mmol) was dissolved in DCM (65 mL), added to the mixture and the reaction was stirred overnight. The solvent was removed by rotary evaporation and the product dissolved in EtOAc (50 mL) and washed with $NaHSO_4$ (2 x 15 mL, 1.33 M), $NaHCO_3$ (2 x 15 mL, saturated), deionised water (3 x 15 mL) and brine (15 mL, saturated). The organic layer was collected, dried with $MgSO_4$, filtered and dried under vacuum. The product was purified by gel permeation chromatography (GPC) column (Bio-beads, 100% DCM). The obtained product was a beige solid (800 mg, 1.8 mmol, 41%). R_f = 0.33 (90:10:1 DCM/MeOH/Et_3N). ^{1}H NMR (400 MHz, $CDCl_3$) δ: 6.81 (br s, N*H*, 1H); 5.12 (br s, N*H*Boc, 1H); 3.30 (q, C*H*$_2$NHCO, *J* = 6.0 Hz, 2H); 3.17 (q, C*H*$_2$NHBoc, *J* = 5.2 Hz, 2H); 2.55 (t, C*H*$_2$N(CH$_3$), *J* = 6.4 Hz, 4H); 2.31 (s, N(C*H*$_3$), 3H); 2.16 (t, C*H*$_2$CONH, *J* = 7.2 Hz, 2H); 1.72 (m, C*H*$_2$CH$_2$N(CH$_3$), 4H); 1.58 (m, C*H*$_2$CH$_2$CONH, 2H); 1.42 (s, C(C*H*$_3$)$_3$, 9H); 1.24-1.22 (m, CH$_2$C*H*$_2$CH$_2$, 20H); 0.86 (t, C*H*$_3$CH$_2$, *J* = 6.8 Hz, 3H). ^{13}C NMR (100 MHz, $CDCl_3$) δ: 176.75 (*C*ONH); 156.92 (O*C*ONH); 77.13 (*C*(CH$_3$)$_3$); 54.13, 53.86 (*C*H$_2$N(CH$_3$)); 39.22 (N(*C*H$_3$)); 36.16 (*C*H$_2$NHCO); 35.52 (CH$_2$CONH); 31.99, 29.74, 29.44 (all *C*H$_2$); 28.42 (C(*C*H$_3$)$_3$); 25.79, 24.84, 24.55,

22.76 (all *C*H_2); 14.20 (*C*H_3CH$_2$). ν_{max} (cm^{-1}) (solid): 3397*m*, 2924*s*, 1691*m*, 1633*m*, 1555*m*, 1514*m*, 1365*m*, 1172*m*, 1049*w*, 722*w*. HRMS: Calcd. $[M+H]^+$ ($C_{26}H_{54}N_3O_3$) *m/z* = 456.4160. Found $[M+H]^+$ *m/z* = 456.4162 (100%).

Boc-Protected C18-DAPMA. Stearic acid (1.00 g, 3.5 mmol) was dissolved in DCM (65 mL). TBTU (1.25 g, 3.9 mmol) and Et_3N (5.4 mL) were added to the mixture and it was stirred for 5 min at room temperature. Mono-Boc-protected DAPMA (860 mg, 3.5 mmol) was dissolved in DCM (65 mL), added to the mixture and the reaction was stirred overnight. The solvent was removed by rotary evaporation and the product dissolved in EtOAc (50 mL) and washed with $NaHSO_4$ (2 x 15 mL, 1.33 M), $NaHCO_3$ (2 x 15 mL, saturated), deionised water (3 x 15 mL) and brine (15 mL, saturated). The organic layer was collected, dried with $MgSO_4$, filtered and dried under vacuum. The product was purified by gel permeation chromatography (GPC) column (Bio-beads, 100% DCM). The obtained product was a light orange gummy solid (1.13 g, 2.2 mmol, 63%). R_f = 0.67 (90:10:1 DCM/MeOH/Et_3N). ^{1}H NMR (400 MHz, $CDCl_3$) δ: 7.15 (br s, N*H*, 1H); 5.47 (br s, N*H*Boc, 1H); 3.30 (q, C*H*$_2$NHCO, *J* = 4.8 Hz, 2H); 3.20 (q, C*H*$_2$NHBoc, *J* = 4.4 Hz, 2H); 3.10 (t, C*H*$_2$N(CH$_3$), *J* = 6.4 Hz, 4H); 2.81 (s, N(C*H*$_3$), 3H); 2.22 (t, C*H*$_2$CONH, *J* = 8.0 Hz, 2H); 1.96 (m, C*H*$_2$CH$_2$N(CH$_3$), 4H); 1.54 (m, C*H*$_2$CH$_2$CONH, 2H); 1.40 (s, C(C*H*$_3$)$_3$, 9H); 1.23-1.21 (m, CH$_2$C*H*$_2$CH$_2$, 28H); 0.85 (t, C*H*$_3$CH$_2$, *J* = 6.8 Hz, 3H). ^{13}C NMR (100 MHz, $CDCl_3$) δ: 176.60 (*C*ONH); 156.93 (O*C*ONH); 77.15 (*C*(CH$_3$)$_3$); 54.14, 53.89 (*C*H$_2$N(CH$_3$)); 39.27 (N(*C*H$_3$)); 36.16 (*C*H$_2$NHCO); 35.59 (CH$_2$CONH); 31.99, 29.78, 29.43 (all *C*H$_2$); 28.42 (C(*C*H$_3$)$_3$); 25.80, 24.86, 24.57, 22.75 (all *C*H$_2$); 14.19 (*C*H$_3$CH$_2$). ν_{max} (cm^{-1}) (solid): 3404*m*, 2917*s*, 1649*m*, 1526*m*, 1467*m*, 1366*m*, 1170*m*, 1054*s*, 722*w*. HRMS: Calcd. $[M+H]^+$ ($C_{30}H_{62}N_3O_3$) *m/z* = 512.4798. Found $[M+H]^+$ *m/z* = 512.4786 (100%).

C14-DAPMA. Boc-protected C14-DAPMA (800 mg, 1.8 mmol) was dissolved in MeOH (50 mL) and HCl gas was applied for approximately 15 seconds. The misture was stirred for 3 hours and the solvent was removed by rotary evaporation. The product was a beige solid (617 mg, 1.4 mmol, 78%). ^{1}H NMR (400 MHz, CD_3OD-d_4) δ: 4.96 (br s, N*H*, 1H); 3.65 (s, N*H*$_2$, 2H); 3.08 (t, C*H*$_2$N(CH$_3$), *J* = 7.2 Hz, 4H); 2.91 (s, NC*H*$_3$, 3H); 2.27 (t, C*H*$_2$CO, J = 7.2 Hz, 2H); 2.17 (m, C*H*$_2$CH$_2$N(CH$_3$), 4H); 2.00 (m, C*H*$_2$CH$_2$CO, 2H); 1.62 (m, C*H*$_2$CH$_2$CO, 2H); 1.30-1.28 (m, CH$_2$C*H*$_2$CH$_2$, 22H); 0.90 (t, C*H*$_3$CH$_2$, *J* = 6.8 Hz, 3H). ^{13}C NMR (100 MHz, CD_3OD-d_4) δ: 177.16 (*C*ONH); 55.29, 54.24 (*C*H$_2$N(CH$_3$)); 40.51 (N(*C*H$_3$)); 37.90 (*C*H$_2$CO); 37.31 (*C*H$_2$NHCO); 36.94 (*C*H$_2$NH$_2$); 33.05, 30.75, 30.46, 26.99, 25.44, 23.72, 23.43 (all *C*H$_2$); 14.51 (*C*H$_3$CH$_2$). ν_{max} (cm^{-1}) (solid): 3352*w*, 3306*w*, 2918*s*, 1638*m*, 1554*m*, 1470*m*, 1090*w*, 722*w*. HRMS: Calcd. $[M+H]^+$ ($C_{21}H_{46}N_3O$) *m/z* = 356.3635. Found $[M+H]^+$ *m/z* = 356.3623 (100%).

C18-DAPMA. Boc-protected C18-DAPMA (800 mg, 1.6 mmol) was dissolved in MeOH (50 mL) and HCl gas was applied for approximately 15 seconds. The mixture was stirred for 3 hours and the solvent was removed by rotary evaporation. The product was a slightly sticky light orange solid (431 mg, 0.89 mmol, 57%). ^{1}H NMR (400 MHz, CD_3OD-d_4) δ: 4.91 (br s, N*H*, 1H); 3.31 (s, NH_2, 2H); 3.08 (t, CH_2N(CH_3), *J* = 7.6 Hz, 4H); 2.90 (s, NCH_3, 3H); 2.25 (t, CH_2CO, *J* = 7.6 Hz, 2H); 2.17-2.09 (m, CH_2CH_2N(CH_3), 4H); 1.99-1.92 (m, CH_2CH_2CONH, 2H); 1.65-1.54 (m, CH_2CH_2CO, 2H); 1.35-1.21 (m, $CH_2CH_2CH_2$, 28H); 0.90 (t, CH_3CH_2, *J* = 6.8 Hz, 3H). ^{13}C NMR (100 MHz, CD_3OD-d_4) δ: 177.89 (*C*ONH); 55.23, 54.26 (*C*H_2N(CH_3)); 40.47 (N(*C*H_3)); 37.90 (*C*H_2NHCO); 37.74 (*C*H_2NH_2); 36.55 (*C*H_2CO); 33.08, 30.81, 30.64, 27.02, 25.22, 23.74, 23.45 (all *C*H_2); 14.50 (*C*H_3CH_2). ν_{max} (cm^{-1}) (solid): 3385*w*, 3243*w*, 2916*s*, 1641*m*, 1543*m*, 1468*m*, 1059*s*, 721*w*. HRMS: Calcd. $[M+H]^+$ ($C_{25}H_{54}N_3O$) *m/z* = 412.4261. Found $[M+H]^+$ *m/z* = 412.4267 (100%).

3. Nile Red Assay[2]

Nile Red assays were performed to determine the critical micellar concentration (CMC) of the binders. A Nile Red solution (2.5 mM) was prepared in ethanol. A blank solution was prepared by placing 1 mL of PBS into a cuvette and adding 1 µL of Nile Red solution. Stock solutions of binder were prepared in PBS at a variety of concentrations starting at 175 µM, 100 µM and 225 µM for C18-DAPMA, C16-DAPMA and C14-DAPMA, respectively. Different amounts of stock solution of binder (1000 µL; 900 µL; 800 µL; 700 µL; 600 µL; 500 µL; 400 µL; 300 µL; 200 µL; 100 µL) were added to cuvettes and the volume was make up to 1 mL with PBS. 1 µL of Nile Red was added to all the cuvettes to give a concentration of 2.5 µM. The fluorescence was recorded with an excitation wavelength of 550 nm and an emission wavelength of 635 nm. The data were obtained in triplicate for each binder. Nile Red assay data are presented in Figs. S1-S3.

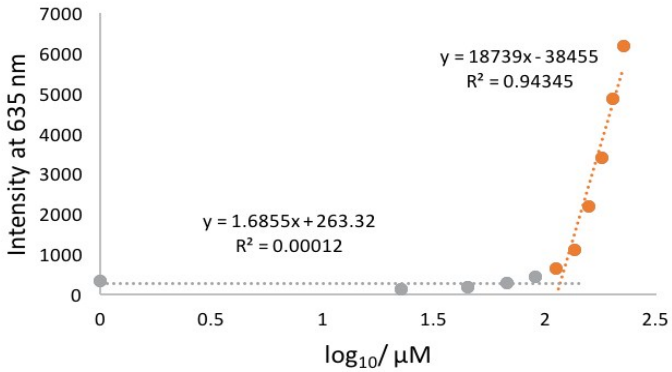

Figure S1. Fluorescence intensity of Nile Red at 635 nm with increasing concentration of C14-DAPMA.

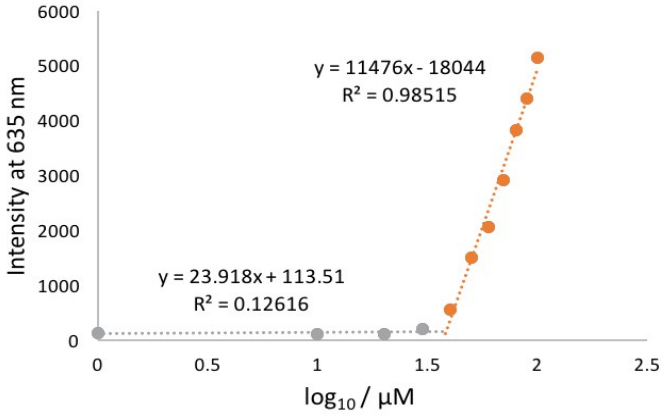

Figure S2. Fluorescence intensity of Nile Red at 635 nm with increasing concentration of C16-DAPMA.

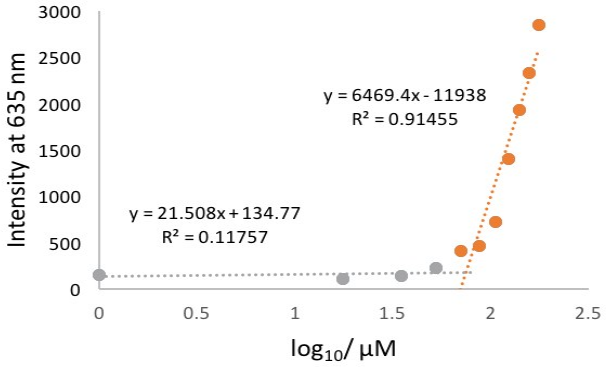

Figure S3. Fluorescence intensity of Nile Red at 635 nm with increasing concentration of C18-DAPMA.

4. Dynamic Light Scattering (DLS)

DLS measurements were carried at 25°C, in triplicate with 11-15 runs per single measurement and the calculated mean values (based on intensity and volume) being used. The samples (1 mL) were prepared in Tris-HCl (10 mM) and NaCl (150 mM) and filtered using a syringe filter PTFE 0.45 µM prior to measurement. DLS data are presented in Figs. S4-S9 as volume distributions.

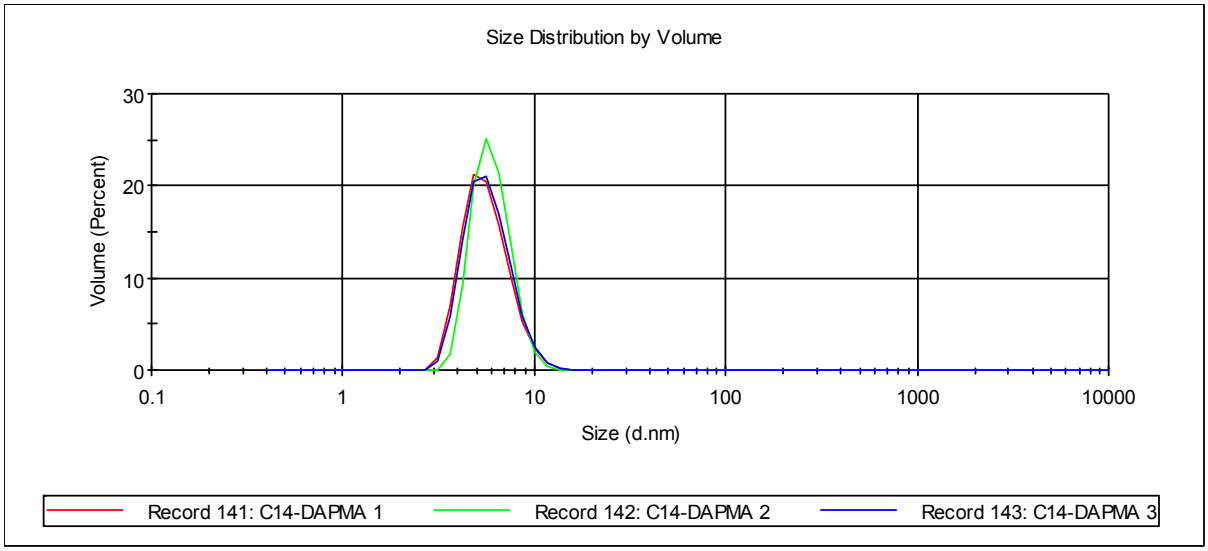

Figure S4. DLS of C14-DAPMA showing size distribution by volume; one trace for each run.

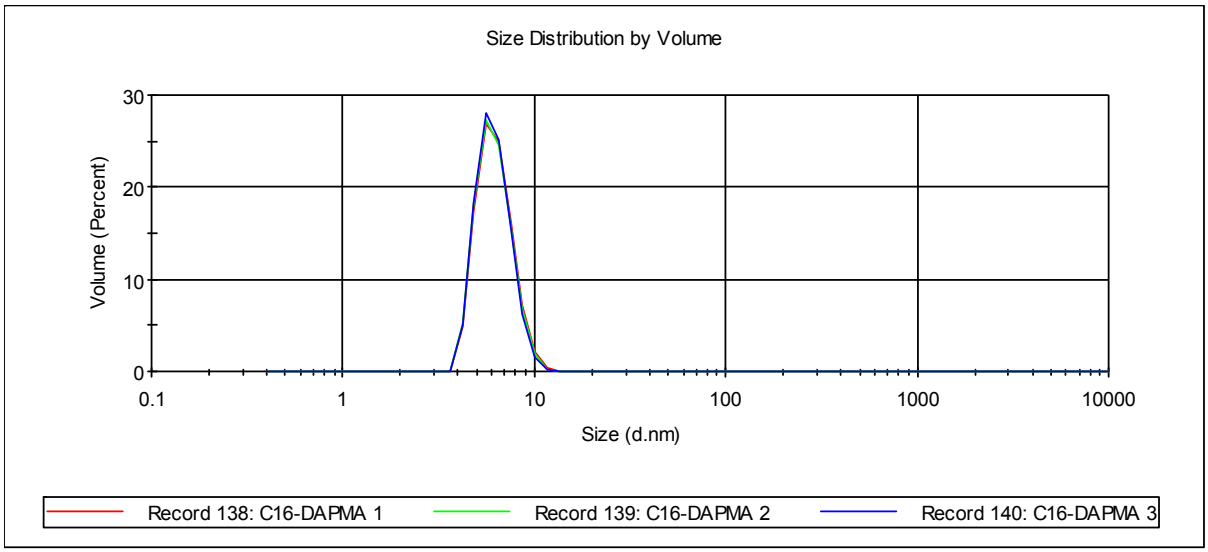

Figure S5. DLS of C16-DAPMA showing size distribution by volume; one trace for each run.

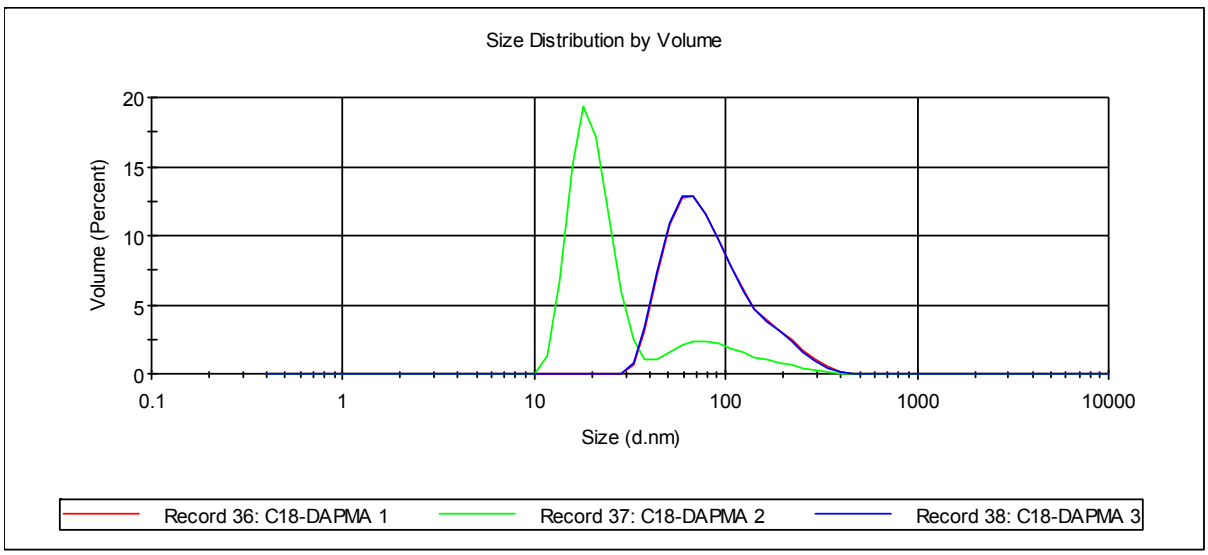

Figure S6. DLS of C18-DAPMA showing size distribution by volume; one trace for each run.

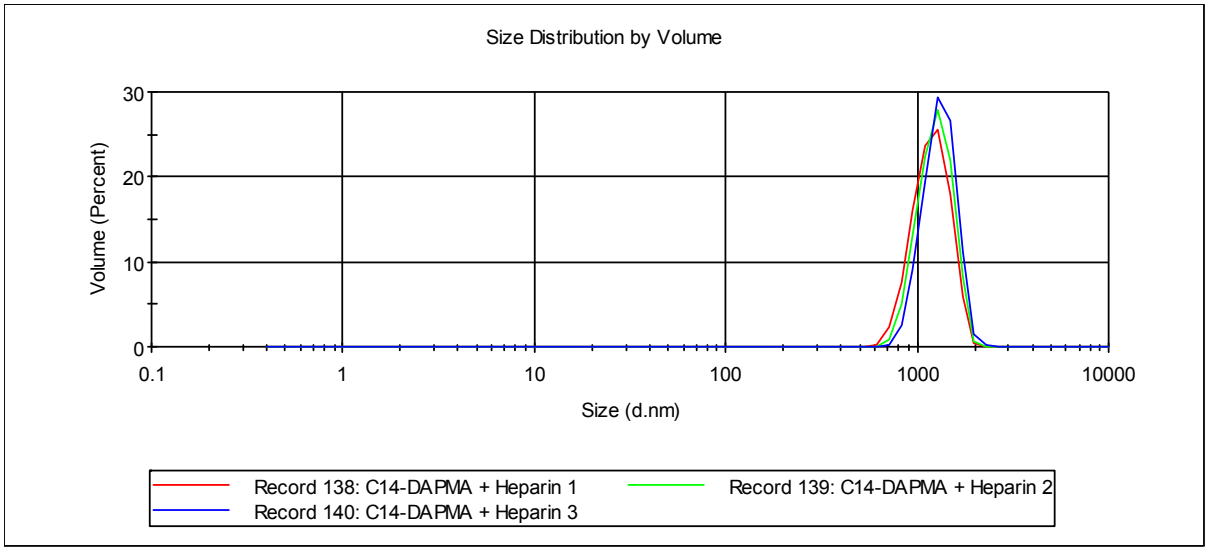

Figure S7. DLS of C14-DAPMA in the presence of heparin showing size distribution by volume; one trace for each run.

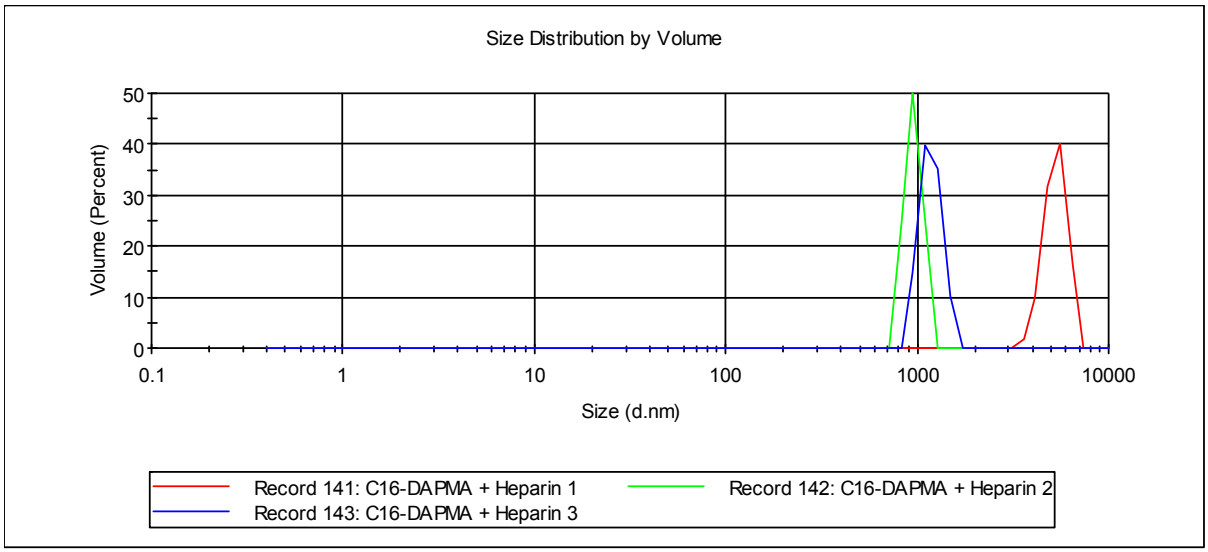

Figure S8. DLS of C16-DAPMA in the presence of heparin showing size distribution by volume; one trace for each run.

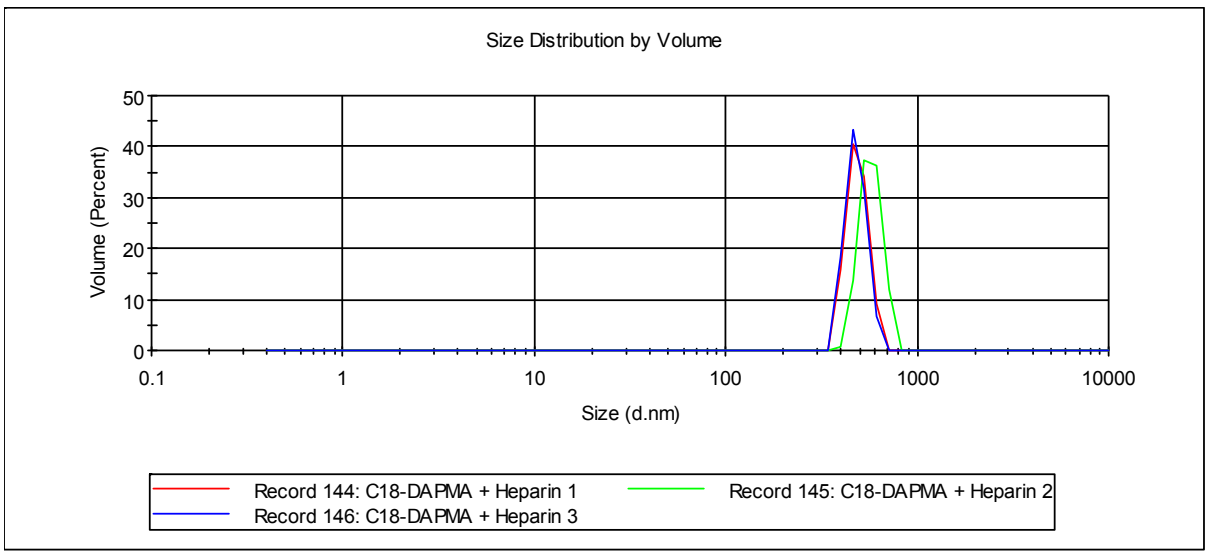

Figure S9.DLS of C18-DAPMA in the presence of heparin showing size distribution by volume; one trace for each run.

5. Mallard Blue (MalB) Assay for Heparin Binding[3]

MalB (25 µM) solution was prepared in Tris-HCl (10 mM) and NaCl (150 mM), wrapped with foil to avoid the contact with direct light and incubated at 50 °C for 24 hours. Heparin (27 µM) was added to the MalB solution, after it cooled down. 2 mL of MalB (25 µM), heparin (27 µM) solution in Tris-HCl (10 mM) and NaCl (150 mM) was placed in a cuvette and titrated with binder stock solution to give a suitable charge ratio for the binder and heparin in the cuvette. Binder stock solution consisted of the solution of MalB and heparin in Tris-HCl (10 mM) and NaCl (150 mM) with a concentration of binder that resulted in a cuvette charge ratio (+ : -) of 0.1, after the addition of 10 µL of binder stock solution. After each addition of the binder stock solution, the cuvette was stirred to ensure the mixing and the absorbance recorded at 615 nm. This procedure was performed in triplicate for each binder. MalB displacement assay data are presented in Figs. S10-S12 as charge ratio versus normalised absorbance at 615 nm.

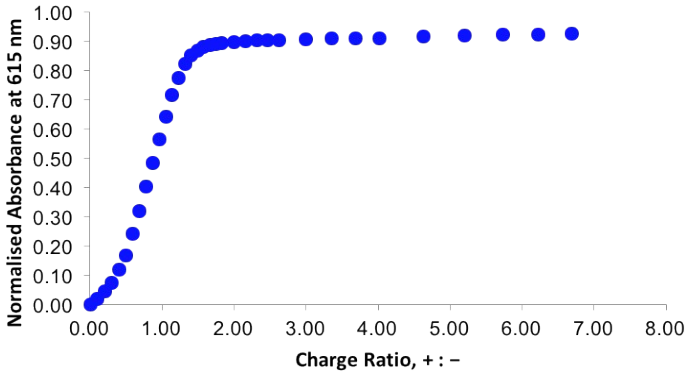

Figure S10. Charge ratio versus normalised absorbance at 615 nm from the MalB displacement assay for C14-DAPMA.

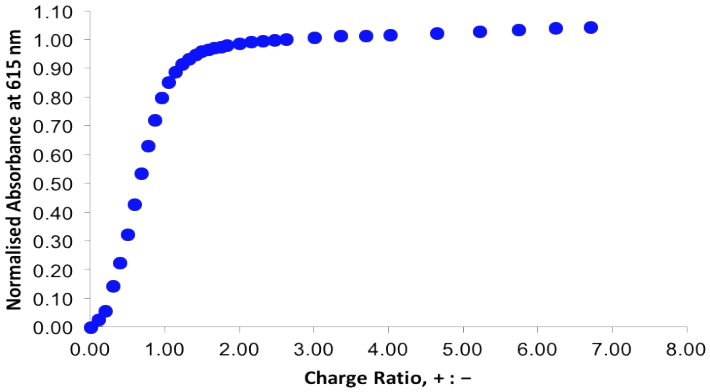

Figure S11. Charge ratio versus normalised absorbance at 615 nm from the MalB displacement assay for C16-DAPMA.

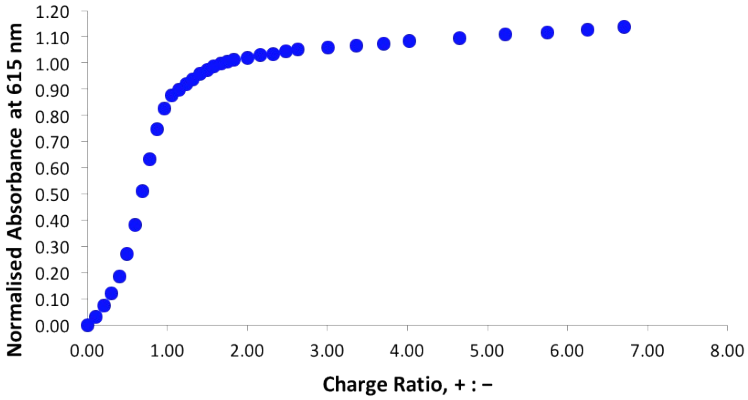

Figure S12. Charge ratio versus normalised absorbance at 615 nm from the MalB displacement assay for C18-DAPMA.

6 Molecular Simulation Methods

Fundamentals of Dissipative Particle Dynamics (DPD) Theory

DPD[4,5] is a particle-based mesoscopic simulation technique commonly employed to investigate the behaviour of surfactants,[6-8] block copolymers and micelles,[9-11] as well as biomolecules[12,13]. The DPD particles (or beads), each representing a group of small molecules or extensive molecular fragments, interact by conservative, dissipative, and random forces, which are pairwise additive. The net force acting on a bead i can be expressed as $\boldsymbol{F}_i = \sum_{j\neq i} (\boldsymbol{F}_{ij}^C + \boldsymbol{F}_{ij}^D + \boldsymbol{F}_{ij}^R)$ and is calculated by summation over all other particles within a certain cutoff radius, r_c, which represents the intrinsic length scale of the DPD model. Let r_c, m, and k_BT be the unit distance, the particle mass, and the thermal energy, respectively.

The conservative force represents the excluded volume interactions between particles i and j in the dimensionless form $\boldsymbol{F}_{ij}^C = a_{ij}\ (1 - r_{ij}\ )\ \hat{\boldsymbol{r}}_{ij}$, where $\boldsymbol{r}_{ij} = \boldsymbol{r}_i - \boldsymbol{r}_j$, $r_{ij} = |\boldsymbol{r}_{ij}|$, $\hat{\boldsymbol{r}}_{ij} = \boldsymbol{r}_{ij}/r_{ij}$, a_{ij} is the maximum repulsion between particles i and j. The dissipative, $\boldsymbol{F}_{ij}^D = -\gamma\ \omega(r_{ij})^2\ (\hat{\boldsymbol{r}}_{ij}\cdot\boldsymbol{v}_{ij})\ \hat{\boldsymbol{r}}_{ij}$, and random forces, $\boldsymbol{F}_{ij}^R = \sigma\ \omega(r_{ij})\ \hat{\boldsymbol{r}}_{ij}\ \zeta/(\Delta t)^{-1/2}$, act as heat sink and source, respectively, and the combined effect of the two forces performs as a thermostat, where γ is a friction coefficient related to the thermal noise amplitude σ via the fluctuation−dissipation theorem, $\sigma^2 = 2\gamma k_BT$, $\omega(r)$ is a weight function, ζ is a normally distributed random variable with zero mean and unit variance that is uncorrelated for different particle pairs, Δt is the time step of an integration scheme, and $\boldsymbol{v}_{ij} = \boldsymbol{v}_i - \boldsymbol{v}_j$ is the relative velocity of the i^{th} and the j^{th} particles. The equations of particle motion, $d\boldsymbol{r}_i/dt = \boldsymbol{v}_i$ and $d\boldsymbol{v}_i/dt = \boldsymbol{F}_i$, are solved using as integration scheme the velocity-Verlet algorithm.

When modeling chains, typically two additional forces are acting between bonded beads: a harmonic spring connecting two adjacent particles *i* and *j* $\boldsymbol{F}_{ij}^{B} = k_b(r_{ij} - r_0)\,\hat{\boldsymbol{r}}_{ij}$, where k_b is a spring constant and r_0 the equilibrium distance between the particles, and $\boldsymbol{F}_{ijz}^{A} = 1/2\; k_\vartheta \sin(\vartheta_0\text{-}\vartheta_0)$, where k_ϑ is a spring constant and ϑ_0 the equilibrium angle between adjacent beads triples *ijz* in a row.

Mesoscale models and simulation details

C14-DAPMA/C16-DAPMA molecules were represented by a flexible chain of beads connected by harmonic springs. The coarse-grained model of C16-DAPMA recently proposed by us[14] was derived by a direct comparison of the appropriate atomistic and DPD pair-pair correlation functions, according to a procedure validated by our group on other, related self-assembling compounds.[15-18] The same computational approach was in turn employed here to obtain the mesoscale topology for C14-DAPMA. As expected due to their structural similarity, each amphiphilic molecule features two different amine moieties (beads N1 and NM), one bead type L, representing the amide group, and a hydrophobic bead C for the alky chain (Figure S13).

Figure S13. Schematic representation of the coarse-grained DPD models of C16-DAPMA (left), C14-DAPMA (right).

Each heparin chain was made by 23 L-iduronic acid (HI) and D-glucosamine (HG) alternating particles sequentially connected through a wormlike chain, adopting the model developed in our previous investigation on dendrimers-heparin binding.[18] Solvent molecules were simulated by single bead types W, and an appropriate number of counterions of a charge of ± 1 were added to preserve charge neutrality and to account for the ionic strength.

In DPD intra- and intermolecular interactions between particles are expressed by the conservative, short-range force $\boldsymbol{F}_{ij}^{C}$, whose intensity is proportional to the pair-repulsive parameter a_{ij}, which accounts for the underlying chemistry of the system considered. In this work, we correlated the interaction energies estimated from atomistic molecular dynamics (MD) simulations to the mesoscale a_{ij} parameter values as proposed for C16-DAPMA and other self-assembling compounds.[15-21] Following this computational recipe described briefly in the following paragraph,

the optimized[14] model of each surfactant type was initially placed close to a heparin chain and the resulting complex was energy minimized to avoid substantial van der Waals overlaps. Each complex was then solvated with an appropriate number of TIP3P[22] water molecules extending at least 20 Å from the solute. A suitable number of counterions (Na^+ and Cl^-) were added to neutralize the system and to mimic the salt conditions. Each system was then relaxed through a combination of steepest descent and conjugate gradient energy minimization steps and equilibrated by MD in the microcanonical ensemble (constant pressure-constant temperature, or NPT, at T = 300 K, P = 1 bar) for 5 ns. These were followed by 30 ns NPT production runs using an integration time step for the equations of motion of 1 fs. The Particle Mesh Ewald technique was used to treat the system electrostatics.[23] The interaction energies between the system molecular constituents were estimated using the Molecular Mechanics/Poisson-Boltzmann Surface Area (MM/PBSA) methodology[24] on a single MD production trajectory of each complex. All of the MD simulations were carried out using AMBER 14[25] platform by applying the *ff14SB* and the *gaff* force field[26] working in our own CPU/GPU hybrid cluster.

Once obtained, the atomistic interaction energies were rescaled onto the corresponding mesoscale segments adapting the procedure described in detail elsewhere.[21] To accomplish this task, two reference values have to be selected. The self-repulsive interaction parameter for water a_{WW} was set equal to 25 k_BT/r_c to fit the isothermal compressibility of water at a dimensionless bead density ρ of 3.[1] The maximum level of hydrophobic repulsion was captured by setting the interaction parameter a_{ij} between the water bead W and the alkyl tail bead C as 80 k_BT/r_c. The counterions were set to have the interaction parameters of water.[24] Accordingly, the conservative DPD interaction parameters a_{ij} are listed in Table S1.

Table S1. DPD bead-bead interaction parameters a_{ij} (in units of k_BT/r_c) used in this work.

a_{ij}	C	L	N1	NM	W	HI	HG
C	26						
L	48	29					
N1	74	33	39				
NM	77	36	38	41			
W	80	34	24	26	25		
HI	62	31	18	35	20	60	
HG	60	27	15	38	18	63	65

All simulations were performed in 3D-periodic cubic boxes of 40^3 r_c^3. The proper number of C16-DAPMA, C14-DAPMA, and heparin molecules was added to the simulation box in order to parallel experimental relevant concentrations and, when appropriate, binder:heparin charge ratio. Unless otherwise stated, in all DPD studies the following reduced units were used: r_c is the unit of length, m is the mass of a DPD particle, and k_BT is the unit of energy. Simulations were carried with a time step of Δt = 0.04 $(k_BT/m)^{-1/2} r_c$ and a simulation period of 5 x 10^5 steps or longer until stabilization occurred.

7 Small Angle X-Ray Scattering (SAXS)

A sample of C16-DAPMA with heparin was prepared by mixing 10 µl of C16-DAPMA (7.36 mg/ml) in Tris-HCl (10 mM) and NaCl (150 mM) with 10 µl of heparin (2.64 mg/ml) also in Tris-HCl (10 mM) and NaCl (150 mM). The sample formed a white precipitate and the SAXS was measured from the precipitate. C14-DAPMA with heparin was prepared by mixing 15 µl of C14-DAPMA (7.08 mg/ml) in Tris-HCl (10 mM) and NaCl (150 mM) with 15 µl of heparin (2.92 mg/ml) in Tris-HCl (10 mM) and NaCl (150 mM). The sample formed a white precipitate and the SAXS was measured from the precipitate.

The wet precipitate was sealed between two Kapton foils during the SAXS measurements. The sample environment was evacuated in order to reduce the scattering from air. The final spot size at the sample position was roughly 1 mm in diameter. The scattered intensity was collected using a Hi-Star 2D area detector (Bruker). Sample-to-detector distance was 0.59 m, and silver behenate standard sample was used for calibration of the length of the scattering vector q. One-dimensional SAXS data were obtained by azimuthally averaging the 2D scattering data. The magnitude of the scattering vector q is given by $q = \frac{4\pi \sin(\theta)}{\lambda}$, where 2θ is the scattering angle.

Figure S14 shows the TEM image of C16-DAPMA (a) binding to heparin, where it is possible to distinguish the crystal projection viewed along the [110] zone axis (b, left). Analysing the line profile over the crystal projection (marked in red) yields an average period (ap) of 4.6 ± 0.3 nm, which corresponds to a fcc lattice constant (a = 3ap/$\sqrt{3}$) of 8.0 nm for C16-DAPMA. Calculating a fast Fourier transform (Figure S14b inset) from the crystalline area (Figure S14b) and filtering the inverse Fourier transform from selected Fourier components, yields an image that represents the unit cell of

the crystal viewed along the [110] zone axis (Figure S14c, left). This can be also confirmed by overlaying the image and a model of the unit cell (Figure S14c, middle) shown in Figure S14c, right.

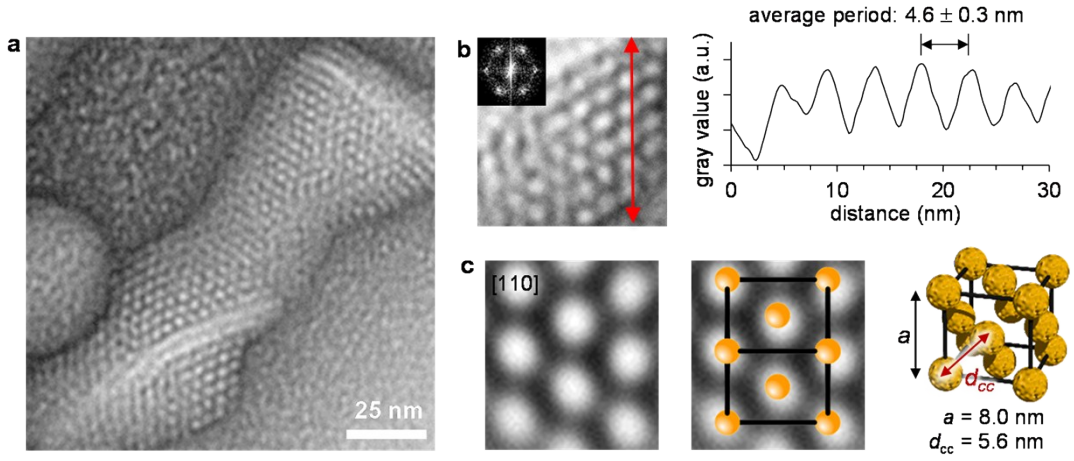

Figure S14. (a) TEM image of C16-DAPMA heparin complex. (b) A crystalline area (left, inset: fast Fourier transform) and a line profile analysis (right) along the red line. c) Filtered inverse Fourier transform from selected Fourier components (left), overlay of the image and fcc unit cell (middle) and model of the fcc unit cell with key dimension (right). Micelles shown in yellow, diameter reduced for clarity.

8. References

1. L. E. Fechner, B. Albanyan, V. M. P. Vieira, E. Laurini, P. Posocco, S. Pricl and D. K. Smith, *Chem. Sci.* 2016, **7**, 4653-4659.
2. M. C. A. Stuart, J. C. Van De Pas and J. B. F. N. Engberts, *J. Phys. Org. Chem.*, 2005, **18**, 929–934.
3. S. M. Bromfield, P. Posocco, M. Fermeglia, S. Pricl, J. Rodríguez-López and D. K. Smith, *Chem. Commun.*, 2013, **49**, 4830–4832.
4. R. D. Groot and P. B. Warren, *J. Chem. Phys.*, 1997, **107**, 4423-4435.
5. I. V. Pivkin, B. Caswell and G. E. Karniadakis, in *Rev. Comput. Chem.*, ed. K. B. Lipkowitz, John Wiley & Sons, Inc., 2011, vol. 27, pp. 85-110.
6. P. Posocco, A. Perazzo, V. Preziosi, E. Laurini, S. Pricl and S. Guido, *RSC Adv.*, 2016, **6**, 4723-4729.
7. A. Vishnyakov, M.-T. Lee and A. V. Neimark, *J. Phys. Chem. Lett.*, 2013, **4**, 797-802.
8. C. Dai, M. Du, M. Zhao, Q. You, B. Guan, X. Wang and P. Liu, *J. Phys. Chem. B*, 2013, **117**, 9922-9928.
9. P. Posocco, Y. M. Hassan, I. Barandiaran, G. Kortaberria, S. Pricl and M. Fermeglia, *J. Phys. Chem. C*, 2016, **120**, 7403-7411.
10. Z. Posel, P. Posocco, M. Fermeglia, M. Lisal and S. Pricl, *Soft Matter*, 2013, **9**, 2936-2946.

11. C. Soto-Figueroa, M.-d.-R. Rodríguez-Hidalgo, J.-M. Martínez-Magadán and L. Vicente, *Macromolecules*, 2008, **41**, 3297-3304.
12. A. Vishnyakov, D. S. Talaga and A. V. Neimark, *J. Phys. Chem. Lett.*, 2012, **3**, 3081-3087.
13. P. Posocco, S. Pricl, S. Jones, A. Barnard and D. K. Smith, *Chem. Sci.*, 2010, **1**, 393-404.
14. L. E. Fechner, B. Albanyan, V. M. P. Vieira, E. Laurini, P. Posocco, S. Pricl and D. K. Smith, *Chem. Sci.*, 2016, **7**, 4653-4659.
15. T. Wei, C. Chen, J. Liu, C. Liu, P. Posocco, X. Liu, Q. Cheng, S. Huo, Z. Liang, M. Fermeglia, S. Pricl, X.-J. Liang, P. Rocchi and L. Peng, *Proc. Natl. Acad. Sci. USA*, 2015, **112**, 2978-2983.
16. X. Liu, J. Zhou, T. Yu, C. Chen, Q. Cheng, K. Sengupta, Y. Huang, H. Li, C. Liu, Y. Wang, P. Posocco, M. Wang, Q. Cui, S. Giorgio, M. Fermeglia, F. Qu, S. Pricl, Y. Shi, Z. Liang, P. Rocchi, J. J. Rossi and L. Peng, *Angew. Chem. Int. Ed.*, 2014, **53**, 11822-11827.
17. A. Barnard, P. Posocco, M. Fermeglia, A. Tschiche, M. Calderon, S. Pricl and D. K. Smith, *Org. Biomol. Chem.*, 2014, **12**, 446-455.
18. S. M. Bromfield, P. Posocco, M. Fermeglia, J. Tolosa, A. Herreros-López, S. Pricl, J. Rodríguez-López and D. K. Smith, *Chem. Eur. J.*, 2014, **20**, 9666-9674.
19. D. J. Welsh, P. Posocco, S. Pricl and D. K. Smith, *Org. Biomol. Chem.*, 2013, **11**, 3177-3186.
20. S. Kala, A. S. Mak, X. Liu, P. Posocco, S. Pricl, L. Peng and A. S. Wong, *J. Med. Chem.*, 2014, **57**, 2634-2642.
21. G. Scocchi, P. Posocco, M. Fermeglia and S. Pricl, *J. Phys. Chem. B*, 2007, **111**, 2143-2151.
22. W. L. Jorgensen, J. Chandrasekhar, J. D. Madura, R. W. Impey and M. L. Klein, *J. Chem. Phys.*, 1983, **79**, 926-935.
23. T. Darden, D. York and L. Pedersen, *J. Chem. Phys.*, 1993, **98**, 10089-10092.
24. V. Tsui and D. A. Case, *Biopolymers*, 2000, **56**, 275-291.
25. D. A. Case, V. Babin, J. T. Berryman, R. M. Betz, Q. Cai, D. S. Cerutti, T. E. Cheatham, T. A. I. Darden, R. E. Duke, H. Gohlke, A. W. Goetz, S. Gusarov, N. Homeyer, P. Janowski, J. Kaus, I. Kolossváry, A. Kovalenko, T. S. Lee, S. LeGrand, T. Luchko, R. Luo, B. Madej, K. M. Merz, F. Paesani, D. R. Roe, A. Roitberg, C. Sagui, R. Salomon-Ferrer, G. Seabra, C. L. Simmerling, W. Smith, J. Swails, R. C. Walker, J. Wang, R. M. Wolf, X. Wu and P. A. Kollman, *AMBER 14, University of California, San Francisco*, 2014.
26. Y. Duan, C. Wu, S. Chowdhury, M. C. Lee, G. Xiong, W. Zhang, R. Yang, P. Cieplak, R. Luo, T. Lee, J. Caldwell, J. Wang and P. Kollman, *J. Comput. Chem.*, 2003, **24**, 1999-2012.
27. X. Fan, N. , S. Phan-Thien, X. W. Chen and T. Y. Ng, *Phys. Fluids*, 2006, **18**, 63102–63110.